



Contents lists available at ScienceDirect

Arabian Journal of Chemistry

journal homepage: www.sciencedirect.com



Original article

# Hierarchical porous biochar for persulfate activation: Non-radical pathway for rapid degradation of organic pollutants

Ya Pang<sup>a</sup>, Jiangfang Yu<sup>b</sup>, Jie Shen<sup>a</sup>, Kun Luo<sup>a,\*</sup>, Xue Li<sup>a</sup>, Yong Song<sup>a</sup>, Min Lei<sup>a</sup>, fangjie Ren<sup>a</sup><sup>a</sup>School of Materials and Environmental Engineering, Changsha University, Changsha 410022, Hunan, China<sup>b</sup>College of Environmental Science and Engineering, Hunan University, Changsha 410082, China

## ARTICLE INFO

## Article history:

Received 29 June 2023

Accepted 3 September 2023

Available online 6 September 2023

## Keywords:

Porous biochar

Persulfate

Non-radical activation

Antibiotics

Environmental remediation

## ABSTRACT

The development of efficient, low-cost, and environmentally friendly catalysts has the potential to significantly enhance the persulfate-based advanced oxidation technology for wastewater treatment. In this study, chitosan gel was utilized as the biomass to be pyrolyzed by two-step pyrolysis method at 600 °C and 800 °C to produce biochar (BC-800). Results from the SEM, TEM, BET, Raman, and XPS characterizations showed that the BC-800 had a surface area of 1748 m<sup>2</sup>/g and a hierarchical pore structure with co-existing macropores, mesopores, and micropores, as well as an obvious graphitic carbon, pyridinic N, and graphitic N configurations. The prepared biochar was found to activate persulfate (PS) for rapid degradation of 2,4-dichlorophenol, with 90% of pollutants removed in 5 min due to the excellent mass transfer facilitated by the abundant pores. Chemical quenching experiments, EPR detection, and electrochemical analysis indicated that the degradation process was triggered by a nonradical pathway, in which the biochar acted as an electron transfer shuttle between the oxidant and pollutant. This electron transfer mechanism not only enabled the degradation system have a wide pH range for application, but it also demonstrated high resistance to inorganic anions in the aquatic environment. This research is expected to enhance the preparation method of hierarchical porous biochar and provide effective technical support for the biochar-activated PS for water purification.

© 2023 The Authors. Published by Elsevier B.V. on behalf of King Saud University. This is an open access article under the CC BY-NC-ND license (<http://creativecommons.org/licenses/by-nc-nd/4.0/>).

## 1. Introduction

Advanced oxidation processes (AOPs) are highly efficient and promising technologies for the treatment of wastewater. Among the various AOPs, the activation of persulfate (PS) (including peroxymonosulfate or peroxydisulfate) to produce reactive oxygen species (ROS) has attracted extensive attention due to the formation of unique sulfate radicals or singlet oxygen, low cost, and the abundant choice of activators (Dong et al., 2022; Dong et al., 2023; Li et al., 2023a; Li et al., 2023b; Yu et al., 2020a). The activator can have significant effect on PS-based AOPs. Metals (such as Fe<sup>2+</sup> and Co<sup>3+</sup>), metal oxides, composite metal oxides (such as MnFe<sub>2</sub>O<sub>4</sub>

and CoFe<sub>2</sub>O<sub>4</sub>), and metal-free carbon materials (such as graphene oxide, reduced graphene oxide, and carbon nanotubes) have been applied to activate PS (Dolatbadi et al., 2023; Li et al., 2022a; Li et al., 2019; Ren et al., 2020; Zhang et al., 2020). Although metal-based activators have been found to be effective, their shortcomings, such as resource scarcity and biotoxicity caused by leached metals, are inevitable. Therefore, more attention is being paid to metal-free carbon materials.

Carbonaceous materials such as zero-dimensional fullerene, nano-diamond, one-dimensional carbon nanotubes, two-dimensional graphene-based materials, and three-dimensional mesoporous carbon, activated carbon, and biochar have been extensively explored for the activation of PS over the past decades (Fu et al., 2022; Indrawirawan et al., 2015; Yu et al., 2019). Among these materials, biochar shows significant potential for large-scale application due to its low cost, adjustable porous structure and surface area, and abundance of oxygen functional groups that can be easily modified (Dai et al., 2021; Song et al., 2022). The use of biochar in environmental remediation not only achieves the effect of resource utilization by using organic solid waste as biomass, but also contributes to carbon reduction. In fact, biochar has been found to exhibit superior activation ability that is comparable with

\* Corresponding author at: School of Materials and Environmental Engineering, Changsha University, Changsha, China.

E-mail address: [Luokun@ccsu.edu.cn](mailto:Luokun@ccsu.edu.cn) (K. Luo).

Peer review under responsibility of King Saud University.



Production and hosting by Elsevier

graphene and metal-based activators (Wang et al., 2019; Yu et al., 2019). The catalytic performance of biochar is highly influenced by its physicochemical properties, such as carbon configuration, porous structure, surface area, and zeta potential. For instance, N-doped biochar synthesized at 900 °C (N-BC-900) showed a degradation rate constant of 39 times higher than that of N-BC-400, which were mainly attributed to the increased graphitic carbon nanosheet and surface area resulting from the increased pyrolysis temperature. And the regulation of physicochemical properties of N-BC could lead to a variation in the activation pathway from radical to nonradical way (Zhu et al., 2018). Besides, in our previous studies, shrimp shell based biochar was found to be a highly effective catalyst for PS activation. It was observed that the porous biochar significantly enhanced the mass transfer ability, and the high surface area allowed for high adsorption of target pollutants on the biochar, thus accelerating the contact between active oxygen substances and the pollutant (Yu et al., 2020b), bringing high degradation efficiency. These findings demonstrate the critical role of designing biochar with a meticulous approach based on the feedstock, target pollutant, and application to obtain an efficient catalyst in biochar-based AOPs.

Compared to homogeneous catalytic systems in AOPs, the use of biochar as a heterogeneous catalyst may reduce the mass transfer efficiency. To overcome this issue, various methods such as modifying the hydrophilicity of biochar, increasing reaction temperature, and enhancing the porous and surface area have been employed as effective strategies (Nguyen et al., 2019; Pang et al., 2018; Zou et al., 2020). Previous research has shown that mesoporous and microporous coexisted biochar (with a reaction rate constant of 0.052 min<sup>-1</sup>) exhibits a slightly higher reaction rate than mesoporous carbon (with a reaction rate constant of 0.048 min<sup>-1</sup>) in PS-based AOPs/2,4-DCP systems (Tang et al., 2018; Yu et al., 2020b). Therefore, preparing a biochar catalyst with an abundant and multi-type porous structure can be an effective approach to improving its performance. The porous property of biochar is mainly influenced by the feedstock and preparation process. Chitosan, the second most abundant biomass after cellulose, contains numerous —OH and —NH<sub>2</sub> groups and is widely used in food, medicine, and industrial wastewater treatment (Strnad and Zemlji, 2023). Additionally, chitosan can absorb 20–35 times of its weight's water. When the water saturated chitosan is dried using vacuum freeze dryer, numerous pores were left. Although acid dissolution of chitosan is the most commonly used method, KOH can be utilized to dissolve chitosan without changing its properties. Moreover, KOH is widely employed in the production of pores in activated carbon and biochar (Dehkhoda et al., 2016; Wang et al., 2022). Hence, using KOH in this study can achieve the dual benefits of dissolving chitosan and introducing pores into biochar.

In this study, to prepare biochar with excellent catalytic properties, chitosan was selected as the biomass, and KOH was utilized as both solvent and pore-forming agent. After dissolving chitosan in KOH solution, the resulting gel was dried using a vacuum freeze dryer. The loosely porous chitosan solid was then subjected to pyrolysis two times to produce biochar. Scanning electron microscopy (SEM) and transmission electron microscopy (TEM), X-ray photoelectron spectroscopy (XPS), Raman and Brunauer Emmett Teller (BET) were employed to characterize its physicochemical properties. The activation ability for PS was evaluated by assessing the degradation of 2,4-dichlorophenol (2,4-DCP), dyes and antibiotics. The effects of pH value, concentration of pollutant, oxidant and biochar, and the co-existing common anions were studied. Furthermore, the activation mechanism was investigated using quenching experiments and electron paramagnetic resonance (EPR) detection. The biochar, which possesses an abundant hierar-

chical porous structure, is expected to serve as a highly effective and environmentally friendly catalyst in PS-based AOPs.

## 2. Materials and methods

### 2.1. Materials

Peroxydisulfate (Na<sub>2</sub>S<sub>2</sub>O<sub>8</sub>), urea, chitosan (deacetylation degree: 80–95%, viscosity: 50–800 mPa·s.), potassium hydroxide, 2,4-dichlorophenol, terramycin, methyl orange, NaCl and NaHCO<sub>3</sub> were purchased from Aladdin Biochemical Co. Ltd. 5,5-dimethyl-1-pyrrolidine N-oxide (DMPO, 97%) and 2,2,6,6-tetramethyl-4-piperidino (TEMP, 98%) were acquired from Sigma-Aldrich (Shanghai, China). Methanol and acetone (chromatography grade) were obtained from Fisher Company Inc (Shanghai, China). Ultrapure water (18.25 MΩ·cm) was utilized to prepare aqueous solutions.

### 2.2. Preparation and characterization of biochar

The chitosan, KOH, urea, and H<sub>2</sub>O were mixed in a weight ratio of 4:11.04:7.68:77.28, and stirred using a magnetic stirring machine for 20–30 min. The resulting mixture was frozen at –20 °C and then thawed at room temperature. This process was repeated three times to dissolve the chitosan and form a homogeneous gel. The gel was then placed in a vacuum drying oven at room temperature to remove any bubbles. Afterward, the gel was dried in a vacuum freezing dryer, resulting in the formation of a material resembling loofa sponge. The material was pyrolyzed at 600 °C for 2 h under nitrogen conditions. The resulting biochar was washed with water to neutral and then dried at 80 °C. The washed biochar was pyrolyzed again under nitrogen conditions for 2 h at 800 °C with a rate of 5 °C min<sup>-1</sup>. The obtained biochar was named as BC-800. For comparison, the dissolved chitosan (loofa sponge-like material) was pyrolyzed under nitrogen for 2 h at 700 °C with a rate of 5 °C min<sup>-1</sup>, and the resulting biochar was named as BC-700.

SEM and TEM were applied to analyze the surface morphologies and structures of the biochar, respectively. The specific surface area, pore size distribution, and pore volume of the biochar were determined using N<sub>2</sub> adsorption–desorption isotherm measurements with an ASAP 2020 HD88 instrument from Micromeritics (USA). And the BET surface area subtract the t-plot micropore area was the surface area of mesoporous pores. And the mesoporous volume was obtained by subtract the t-Plot micropore volume from the total pore volume. X-ray photoelectron spectroscopy (XPS) was used to characterize the elemental compositions of the biochar, and the degree of carbonization was assessed by Raman spectroscopy using a Thermo Scientific DXP 780 instrument (USA).

### 2.3. Experimental procedures

#### 2.3.1. Catalytic degradation of 2,4-DCP

The experiment was carried out in Erlenmeyer flasks on a reciprocating shaker at 120 rpm and a temperature of 27 ± 1.0 °C in the absence of light. The initial pH of the reaction solution was approximately 7.0. The reaction was initiated by adding 1.25 mM PS and 0.12 g/L BC-800 into the reaction solution containing 40 mL of 50 mg/L 2,4-DCP, and the glass vials were capped. Control experiments were conducted using BC-700 as a catalyst under the same conditions. Samples were periodically taken (1 mL) and filtered using a 0.22 μm cellulose-acetate membrane for analysis. The concentration of 2,4-DCP was determined by HPLC (Waters e2695) using a C18 column (5.0 μm, 4.6 mm × 250 mm) and a UV detector set at 286 nm, with a mobile phase of methanol/water = 80/20. Quenching experiments and anti-interference experiments (using Cl<sup>-</sup> and HCO<sub>3</sub><sup>-</sup> as the interfering ions) were conducted by adding

ethanol, methanol, and other anions to the reaction system. All batch experiments were conducted in triplicate, and the mean values were presented. Pseudo-first-order kinetic investigation of 2,4-DCP degradation process was fitted by Langmuir-Hinshelwood model, which expressed as  $\ln C_i/C_0 = kt$ . Where  $C_0$  and  $C_i$  correspond to the 2,4-DCP concentrations at initial state and degradation time of  $t$ , respectively. And  $k$  was the pseudo-first-order rate constant.

### 2.3.2. Electrochemical test

The electrochemical impedance spectroscopy (EIS) performance of biochar samples, BC-800 or BC-700, was evaluated using a CHI 660C electrochemical analyzer (CHI-660C, China). In this experiment, a glassy carbon electrode loaded with biochar was employed as the working electrode. The preparation process involved dissolving 0.012 g of chitosan in 10 mL of 0.1 M HAC solution, followed by the addition of 0.005 g of the prepared biochar. The mixture was sonicated for 3 h to facilitate biochar dispersion. Subsequently, the glassy carbon electrode was rubbed with sandpaper (0.05  $\mu\text{m}$ ), cleaned with acetone, methanol, and distilled water using ultrasonication, and then dried in an oven. Finally, 5–8  $\mu\text{L}$  of the dispersed biochar was dropped onto the surface of the glassy carbon electrode and dried at 37 °C.

## 3. Results and discussion

### 3.1. Characterization of biochar

The SEM image in Fig. 1a shows that BC-800 contains numerous macropores with diameters ranging from 0.3 to 4  $\mu\text{m}$ , while Fig. 1b shows that smaller pores are present on the frame of BC-800. The BET analysis indicates the presence of micropores and mesopores. And the BC-800 has a BET surface area of 1748  $\text{m}^2/\text{g}$ , a total pore volume of 0.976  $\text{cm}^3/\text{g}$ , and an average pore diameter of 2.23 nm (Fig. 2). The mesoporous structure is the dominant feature for BC-800, with a surface area of 1674.9  $\text{m}^2/\text{g}$  and a mesoporous volume of 0.970  $\text{cm}^3/\text{g}$ . The adsorption–desorption isotherm curves demonstrate a typical IV type (Fig. 2a), which is consistent with the mesoporous structure of BC-800, as confirmed by the BET analysis (Fig. 2b). In contrast, BC-700 has a low surface area of 275.23  $\text{m}^2/\text{g}$  and a pore volume of 0.1802  $\text{cm}^3/\text{g}$ . The surface area and pore volume of BC-800 was significant high compared to most other biochar, which are mainly due to the preparation process (Yu et al., 2020b; Ding et al., 2023; Zhang et al., 2015). The use of freeze-drying was found to be an effective method for obtaining a three-dimensional porous structure in chitosan, and the dried chitosan gel was a loofa sponge-like product. During the subsequent pyrolysis process, some of porous structure was preserved and contributed to the formation of macropores, as shown in Fig. 1a. The presence of macropores in BC-800 is an important characteristic that facilitates mass transfer. Furthermore, KOH served not only as a solvent but also as an activating agent for pore formation. Instead of micropores, mesoporous volume accounted for about 99% of the total pore volume in BC-800. This differs from Lee's study, where chitosan, urea, and KOH were mixed and pyrolyzed at 800°C without the use of freeze-drying pre-treatment, resulting in mesoporous volume accounting for only 52% of the total pore volume (Lee et al., 2017). The combination of KOH with freeze-drying was identified as a critical factor in the formation of abundant mesopores in BC-800. Moreover, the two-step pyrolysis process was proved to be essential for the development of pores and the enlargement of pore size by eliminating compounds such as water-soluble and volatile matter, as well as gases such as CO, CO<sub>2</sub>, CH<sub>4</sub>, H<sub>2</sub>, and H<sub>2</sub>S from the biochar. Notably, direct pyrolysis of freeze-dried chitosan at 800°C resulted in the formation of white

solid materials that could dissolve in water and exhibited strong alkalinity. This observation suggests that under high temperature, a significant portion of C in chitosan likely reacted with KOH to generate K<sub>2</sub>CO<sub>3</sub>, K<sub>2</sub>O, and CO<sub>2</sub>.

Furthermore, in order to provide further characterization of the prepared biochar, TEM and Raman analysis were also conducted. TEM images at different magnification scales (Fig. 1c,d) confirmed the multi-porous and smooth structure of the biochar, which was consistent with the SEM results. Moreover, the presence of a typical stripe-like structure was observed in Fig. 1d, which indicated the formation of graphitic carbon (Liu et al., 2018). Additionally, Raman spectroscopy was performed on BC-800 and BC-700 using an excitation wavelength of 532 nm to investigate the defective and graphitic features. As depicted in Fig. 1e, typical D and G peaks were observed at around 1350  $\text{cm}^{-1}$  and 1580  $\text{cm}^{-1}$ , respectively. The D peak, arising from the ring breathing vibration mode of carbon, is commonly considered as the signal of disordered or edge graphite carbon, while the G peak, often resulted from the in-plane vibration mode of sp<sup>2</sup>-hybridized carbon (graphitic carbon) (Kim et al., 2012; Yu et al., 2020b). The ID/IG value, which is commonly used to evaluate the relative degree of defect and graphitization, was 0.982 and 0.967 for BC-700 and BC-800, respectively. The decrease in the ID/IG value indicated that the graphitization degree of the biochar increased with the rising of pyrolysis temperature. This was consistent with the previous results that with the increasing of pyrolysis temperature, the carbon configuration transformed from amorphous to graphitic type, especially when the temperature exceeded 700 °C (Li et al., 2022b; Yuan et al., 2023). And XPS spectrum of C1s (Fig. 1g) also verified the sp<sup>2</sup>-hybridized graphitic carbon (C=C).

The addition of urea served two purposes: first, to significantly undermine the molecular hydrogen bond and hydrophobic interactions of chitosan and raise the critical micelle concentration, thereby promoting chitosan dissolution (Fang et al., 2015; Fang et al., 2017). Second, during pyrolysis, urea acted as a nitrogen source and doped to the biochar. XPS spectrum of BC-800 showed that N elements existed in the biochar with atomic percentage of 7.4% (Fig. 1f). And N1s spectrum presented three peaks, which belong to pyridinic N, pyrrolic N and graphitic N (Fig. 1h) (Xu et al., 2016; Zhong et al., 2021). Doping nitrogen has been shown to be an effective way to modulate the electronic properties of the carbon framework and improve the catalytic performance of biochar (Liu et al., 2022; Li et al., 2020). As for O 1s spectrum, C=O and C–O were the main chemical state.

### 3.2. Catalytic performances of biochar for 2,4-DCP degradation

Firstly, adsorption and catalytic experiments of BC-800 and BC-700 were conducted. Specifically, 40 mL of 50 mg/L 2,4-DCP solution was treated by adding 0.75 mM PS and different biochar with a pH value of 7. As shown in Fig. 3a, single 0.005 g BC-800 could remove 56% of 2,4-DCP. After Adding PS, the removal efficiency was close to 98% (experiments showed that single PS had negligible ability to remove 2,4-DCP), indicating the excellent catalytic ability of BC-800 for PS. Moreover, the catalytic speed was rapid, with 90% of 2,4-DCP removed in the first 5 min, and complete degradation of 2,4-DCP could be reached in about 30 min. The reaction rate constants based on pseudo first order kinetics were  $k = 0.0577 \text{ min}^{-1}$  ( $r^2 = 0.928$ ) for adding 0.005 g BC-800, which was higher than mesoporous carbon based PS-2,4-DCP AOPs system (Tang et al., 2018). The rapid degradation speed was very useful for practical applications. Compared with BC-800, the catalytic efficiency and speed of BC-700 ( $k = 0.0271 \text{ min}^{-1}$   $r^2 = 0.956$ ) were inferior (Fig. 3b). As verified by BET surface area and pore size analysis, the surface area of BC-800 (1748  $\text{m}^2/\text{g}$ ) was 6.3 times that of BC-700, and the graphitization degree of BC-800 was higher than

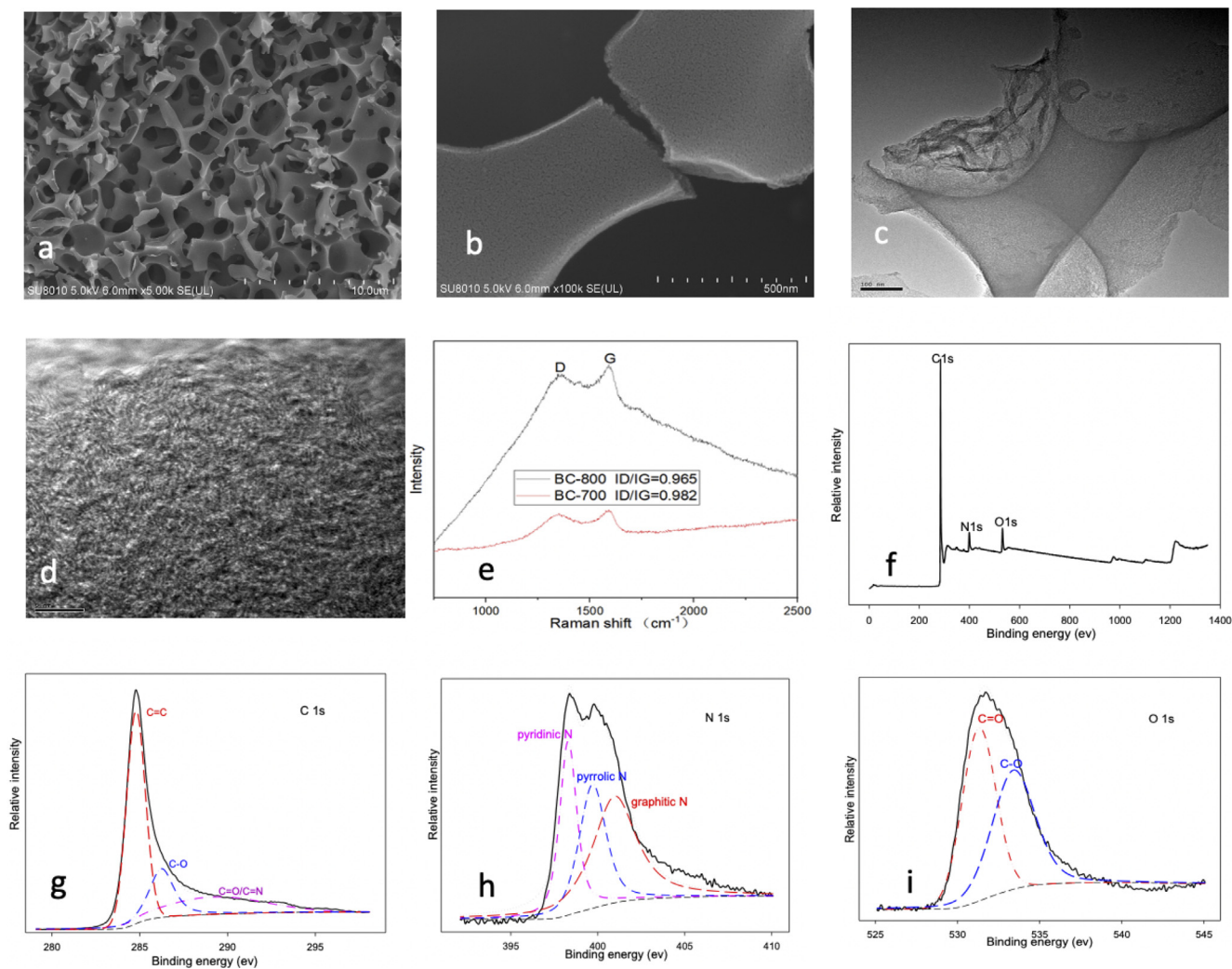


Fig. 1. SEM images of BC-800 (a,b), TEM images of BC-800 (c,d), Raman results of BC-800 and BC-700 (e), XPS full spectrum (f), C1s peaks (g), N1s peaks (h) and O1s peaks (i) of BC-800.

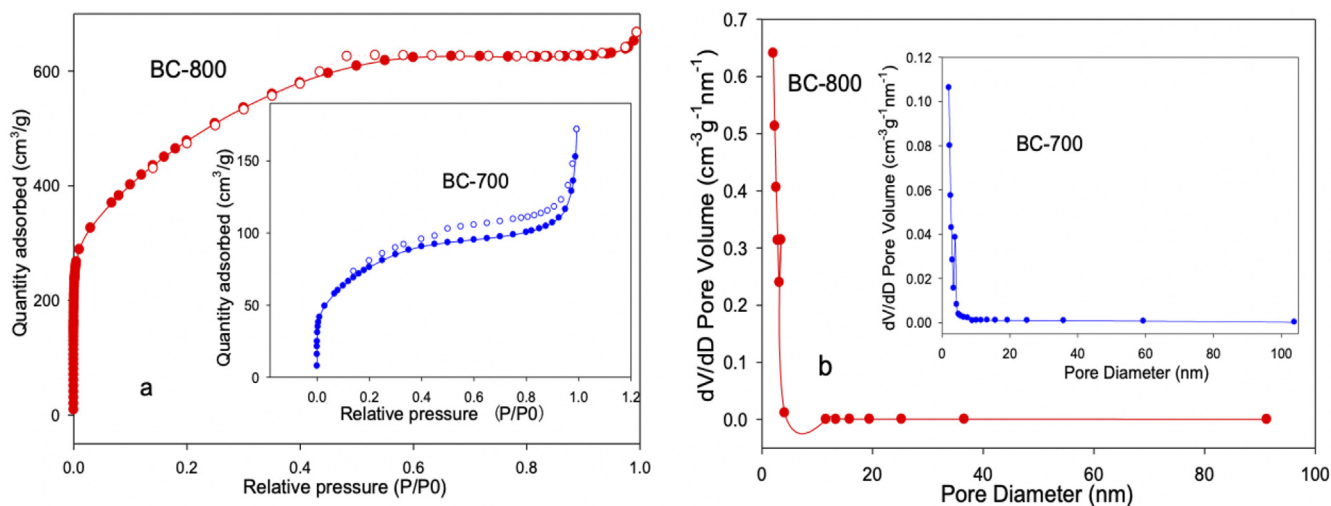


Fig. 2. N<sub>2</sub> adsorption/desorption isotherm and pore distribution of BC-800 and BC-700.

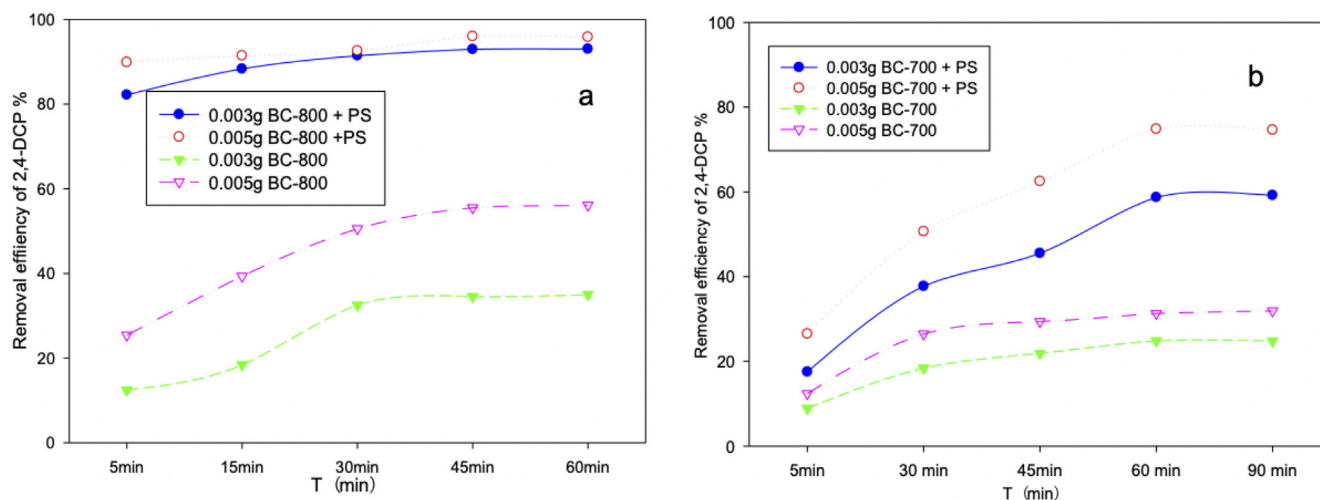


Fig. 3. The adsorption and catalytic performances of BC-800 (a) and BC-700 (b).

that of BC-700. Therefore, BC-800 was used for further investigation.

### 3.3. The effect of operating parameters

Operation parameters including pH, the concentration of BC-800, PS, and pollutant, were investigated. Fig. 4a and 4b showed that with the reduction of BC-800 or the increasing of 2,4-DCP, the removal efficiency decreased. Since BC-800 mainly acted as an activator (the mechanism study indicated that the activation process was a non-radical pathway), PS could not be fully activated under insufficient BC-800, and subsequently, the degradation of 2,4-DCP would decrease correspondingly. A similar explanation could be used for the effect of 2,4-DCP concentration, and the degradation rate constant decreased from  $0.0774$  to  $0.0216 \text{ min}^{-1}$  ( $r^2$  greater than  $0.914$ ) with the increasing of 2,4-DCP from 30 to 100 mg/L. The rapid degradation of 2,4-DCP was beneficial for practical applications. The distinctive porous structure may have contributed to the fast degradation. As verified by SEM and BET results, macroporous-mesoporous-microporous coexisted in BC-800, and mesoporous took up more than 90% of the proportion. Mass transfer efficiency could be significantly improved due to the abundant macroporous and mesoporous structure. Besides mass transfer, the nanoconfined space (nanopore) could enrich reactants (Zhang et al., 2021). As demonstrated in Fig. 3, BC-800 was able to adsorb 2,4-DCP, prolonging the residence time of reactants on the catalyst surface. The generated reactive oxygen substances could quickly contact and degrade 2,4-DCP, leading to rapid degradation performances. In our previous study, shrimp shell biochar with a hierarchical porous structure also exhibited fast adsorption and catalytic performances due to the increased mass transfer ability. Therefore, preparing biochar with different porous structures may be a feasible strategy for improving its performance. Fig. 4c indicated that exceeding PS would not inhibit the degradation reaction, mainly due to the non-radical activation process, which avoids the self-quenching of sulfate radicals by PS. As shown in Fig. 4d, this degradation system had a wide pH suitability, and the following experiments were done without adjusting the pH value. Besides excellent pH compatibility, the catalytic system could maintain high removal efficiency for 2,4-DCP under high concentrations of commonly existing anions. The anti-interference experimental results were presented in Fig. 4e, after adding  $\text{Cl}^{-1}$  and  $\text{HCO}_3^{-1}$  with the concentration of 10 and 400 times that of PS, the removal efficiency of 2,4-DCP was still higher than 90%. The

wide pH adaptability and good anti-interference performance indicated that this catalytic system could be used for most wastewater. After usage, the biochar was simply washed with water and ethanol, and could be reused three times with activation efficiency of initial 80%. When the BC-800/PS was used to treat dye (methyl orange) and antibiotics (oxytetracycline), the removal efficiency of antibiotics was inferior to that of the dye, as presented in Fig. 4f. It is possible that the chemical stability of oxytetracycline ( $\text{C}_{22}\text{H}_{24}\text{N}_2\text{O}_9$ ) was stronger than that of methyl orange ( $\text{C}_{14}\text{H}_{14}\text{N}_3\text{SO}_3\text{Na}$ ) in this system, and methyl orange was more inclined to donate electrons to BC-800/PS, leading to a high degradation efficiency.

### 3.4. Activation mechanism investigation

Firstly, the activation pathway was investigated using quenching experiments and EPR detection. Ethanol and methanol, which had high quenching ability for both  $\cdot\text{OH}$  and  $\text{SO}_4\cdot^-$ , were used to detect the two free radicals. As shown in Fig. 5a, no inhibition effect was observed after adding ethanol and methanol ( $C_{\text{methanol}}$  or  $C_{\text{ethanol/PS}} = 300$  or 500) to the catalytic system. EPR detection using 5,5-dimethyl-1-pyrroline N-oxide (DMPO) as a trapping agent also verified the absence of both  $\cdot\text{OH}$  and  $\text{SO}_4\cdot^-$ . These results suggested that the non-radical pathway is responsible for the degradation of 2,4-DCP in this catalytic system. To further investigate the non-radical pathway, a quenching experiment using  $\text{NaN}_3$  ( $k^1\text{O}_2 + \text{sodium azide} = 2 \times 10^9 \text{ M}^{-1}\text{s}^{-1}$ ) as a quenching solvent and EPR detection using 2,2,6,6-tetramethylpiperidine-1-oxyl (TEMP) as a trapping agent were conducted (Yu et al., 2020a). The absence of  $^1\text{O}_2$  was observed, indicating that the  $^1\text{O}_2$ -dominated degradation mechanism could be excluded. Notably, unlike the signal of DMPO-OH or DMPO- $\text{SO}_4\cdot^-$  or TEMPO, a characteristic signal of DMPOX adducts (5,5-dimethyl-2-pyrroline-N-oxyl) was detected in the catalytic degradation system (Fig. 5b). According to the previous studies, there were three ways to produce DMPOX: the first way is oxidation of DMPO-OH by a large amount of  $\cdot\text{OH}$  and  $\text{SO}_4\cdot^-$ , the second way involved the reaction between  $^1\text{O}_2$  and DMPO. However, both these pathways were eliminated due to the exclusion of the radical pathway and  $^1\text{O}_2$ -based non-radical pathway. The third way is a reaction between DMPO and carbon surface-bound oxidative complexes (Fontmorin et al., 2016; Jiang et al., 2018; Li et al., 2018). As verified by TEM and Raman results, BC-800 had a good graphitization degree, which was beneficial for electron transfer. Carbon catalysts used as charge-transfer media-

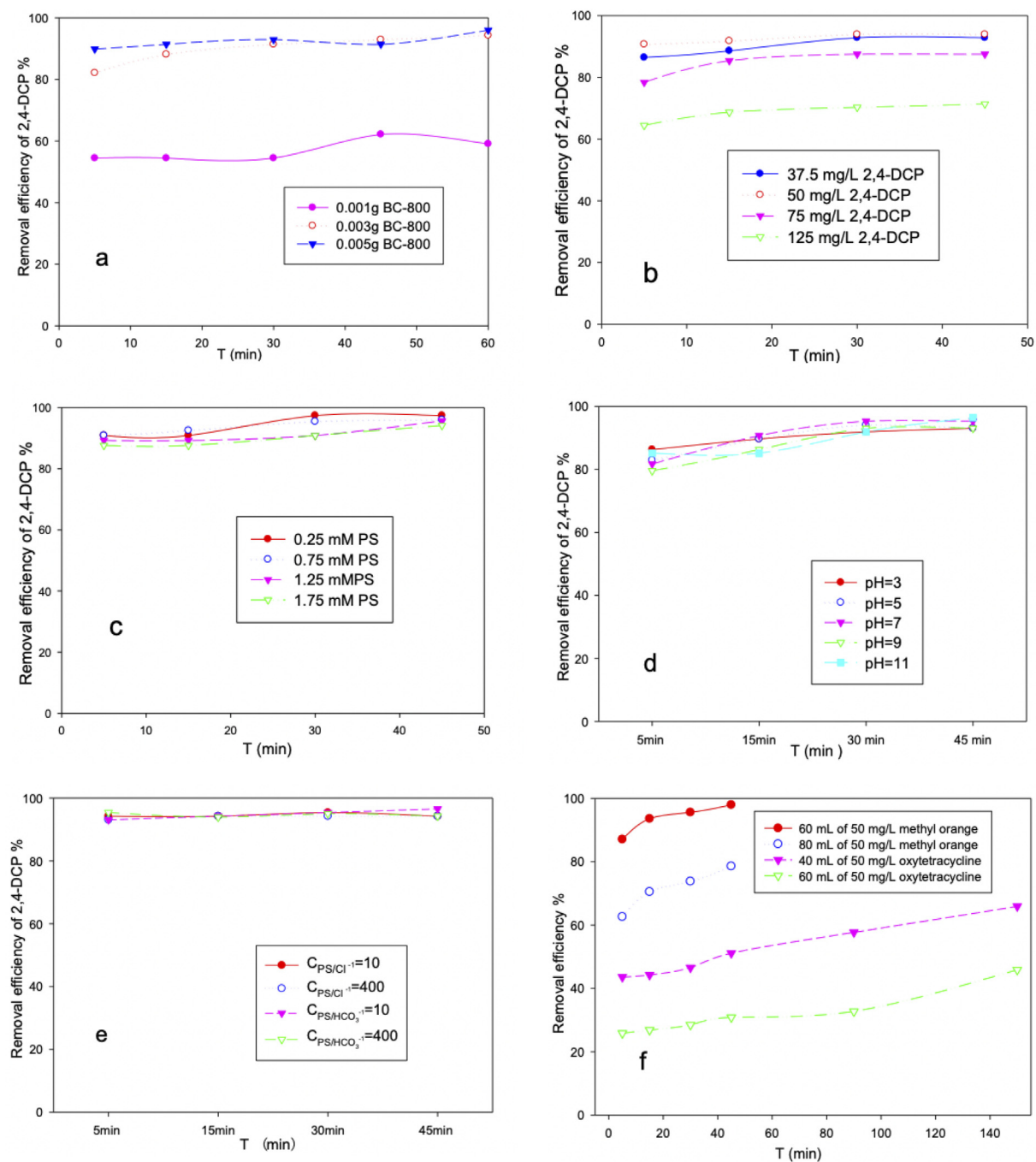


**Fig. 4.** Factorial effects for the catalytic degradation of 2,4-DCP, BC-800 concentration (a), 2,4-DCP concentration (b), PS concentration (c), pH value (d), co-existing anion concentration (e), and effect of degradation of methyl orange and oxytetracycline (f). (Unless otherwise stated, the reaction conditions were based on: BC-800 = 0.12 g/L; PS = 1.25 mM; 2,4-DCP = 50 mg/L; pH = 7; and T = 25 °C).

tors to promote electron transport from the pollutants to PS were reported by many researchers (Xi et al., 2021; Yu et al., 2020b; Zhong et al., 2021). A similar mechanism where BC-800 acted as an electron transfer medium to trigger the non-radical pathway may dominate the 2,4-DCP oxidation in the BC-800/PS system. As presented in Fig. 5c of the EIS results, the charge-transfer resistance of BC-800 significantly reduced compared with BC-700, indicating the excellent charge transfer capacity. In a contrast experiment (Fig. 5d), where BC-800 and PS were first mixed, 125 mg/L of 2,4-DCP was added to the BC-800/PS system at different times, the removal efficiency of 2,4-DCP was almost the same for the three batches of experiments. If BC-800 and PS reacted

and produced radicals or active complexes, the removal efficiency of 2,4-DCP would decrease with the increasing of addition time, because the lifetime of radicals or active complexes was limited. Therefore, based on the these analysis, an electron transfer pathway was verified to dominate the degradation of 2,4-DCP, where BC-800 acted as an electron transfer medium, and the degradation could only be triggered in the presence of BC-800, PS, and 2,4-DCP as shown in Fig. 6. Regarding the formation of DMPOX, during the degradation of 2,4-DCP in the BC-800/PS system, it was possible that BC-800 could transform to an oxidative state (BCox-800 represented the oxidation state of BC-800), and DMPO reacted with BCox-800 to produce DMPOX.

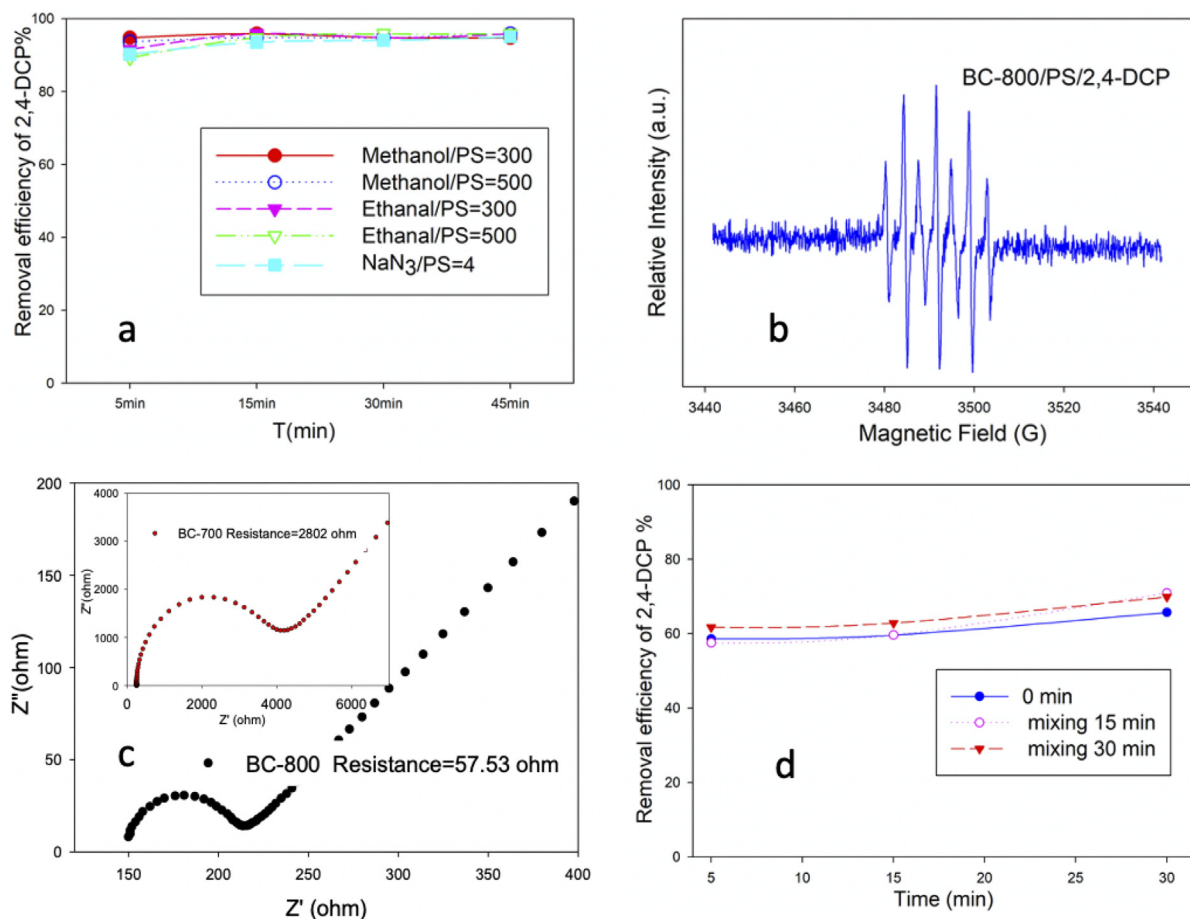


**Fig. 5.** Quenching experiments by different quenching reagent (a), the EPR detection spectrum of BC-800/2,4-DCP/PS system (b), electrochemical impedance spectroscopy (EIS) results of BC-800 and BC-700 (c), the different adding time of 2,4-DCP to BC-800/PS system (d).

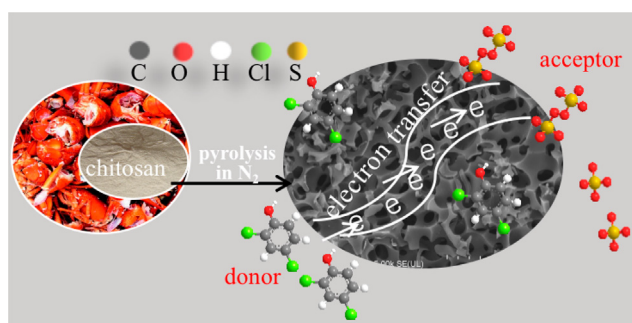


**Fig. 6.** Mechanism diagram of activation pathway in BC-800 /PS /2,4-DCP system.

#### 4. Conclusion

In this study, hierarchical porous biochar with high surface area, and excellent graphitic carbon configuration was prepared through a two-step pyrolysis method. This biochar showed effective ability and rapid rates for PS activation, and 90% 2,4-DCP could be degraded in 5 min. The batch experiments showed that the catalytic degradation performances maintained high even under a wide pH range of 3–11 and the coexistence of high concentrations of Cl<sup>-1</sup> and HCO<sub>3</sub><sup>-1</sup>, indicating good anti-interference properties. Additionally, activation mechanism studies suggested that a non-radical pathway, that biochar acted as an electron transfer shuttle between the oxidant and pollutant, where the degradation process was triggered only in the coexistence of biochar, PS, and 2,4-DCP.

This study not only provided a simple method for the preparation of effective biochar catalyst in AOP, but also suggested regulating porosity and carbon configuration might be a purposeful way in the carbon catalyst/PS AOP system.

#### Declaration of Competing Interest

The authors declare that they have no known competing financial interests or personal relationships that could have appeared to influence the work reported in this paper.

#### Acknowledgments

The authors greatly appreciate the financial support from The science and technology innovation Program of Hunan Province (2022RC1129), Natural Science Foundation of Hunan Province (2022JJ30634), and the Training Program for Excellent Young Innovators of Changsha (kq2206050) and Changsha Municipal Natural Science Foundation (kq2202169), the National Natural Science Foundation of China (52200194, 52000013), the Research Project of Education Department of Hunan Province of China (21B0767, 22A0593, 22A0594).

#### References

- Dai, L. et al., 2021. Tuning oxygenated functional groups on biochar for water pollution control: a critical review. *J. Hazard. Mater.* 420, 126547–126568.
- Dehkhoa, A.M. et al., 2016. A novel method to tailor the porous structure of KOH-activated biochar and its application in capacitive deionization and energy storage. *Biomass Bioenergy* 87, 107–121.

- Ding, H. et al., 2023. Regeneration of methylene blue-saturated biochar by synergistic effect of H<sub>2</sub>O<sub>2</sub> desorption and peroxymonosulfate degradation. *Chemosphere* 316, 137766.
- Dolatabadi, M. et al., 2023. Accelerated degradation of groundwater-containing malathion using persulfate activated magnetic Fe<sub>3</sub>O<sub>4</sub>/graphene oxide nanocomposite for advanced water treatment. *Arab. J. Chem.* 16, 104424.
- Dong, C. et al., 2022. A comprehensive review on reactive oxygen species (ROS) in advanced oxidation processes (AOPs). *Chemosphere* 308, 136205–136220.
- Dong, Z.J. et al., 2023. Fe (II)-activated persulfate oxidation effectively degrades iodoform in water: influential factors and kinetics analysis. *Arab. J. Chem.* 13, 5009–5017.
- Fang, Y. et al., 2015. Intermolecular interaction and the extended wormlike chain conformation of chitin in NaOH/Urea aqueous solution. *Biomacromolecules* 16, 1410–1417.
- Fang, Y. et al., 2017. Recyclable universal solvents for chitin to chitosan with various degrees of acetylation and construction of robust hydrogels. *ACS Sustain. Chem. Eng.* 5, 2725–2733.
- Fontmorin, J.M. et al., 2016. Stability of 5,5-dimethyl-1-pyrroline-N-oxide as a spin-trap for quantification of hydroxyl radicals in processes based on Fenton reaction. *Water Res.* 99, 24–32.
- Fu, Q. et al., 2022. Porous carbon nano-sheets as excellent carbocatalysts for organic pollutant removal via persulfate activation: the role of the sp<sup>2</sup>/sp<sup>3</sup> carbon ratio. *Environ. Sci. Nano* 9, 1748–1758.
- Indrawirawan, S. et al., 2015. Nanocarbons in different structural dimensions (0–3D) for phenol adsorption and metal-free catalytic oxidation. *Appl. Catal. B Environ.* 179, 352–362.
- Jiang, L. et al., 2018. Oxidation of Rhodamine B by persulfate activated with porous carbon aerogel through a non-radical mechanism. *J. Hazard. Mater.* 358, 53–61.
- Kim, K.H. et al., 2012. Influence of pyrolysis temperature on physicochemical properties of biochar obtained from the fast pyrolysis of pitch pine (*pinus rigida*). *Bioresour. Technol.* 118, 158–162.
- Lee, D.W. et al., 2017. Straightforward synthesis of hierarchically porous nitrogen-doped carbon via pyrolysis of Chitosan/Urea/KOH mixtures and its application as a support for formic acid dehydrogenation catalysts. *ACS Sustain. Chem. Eng.* 5 (11), 9935–9944.
- Li, X.N. et al., 2018. Single cobalt atoms anchored on porous N-Doped graphene with dual reaction sites for efficient fenton-like catalysis. *J. Am. Chem. Soc.* 140, 12469–12475.
- Li, W. et al., 2019. Removal of ciprofloxacin by persulfate activation with CuO: A pH-dependent mechanism. *Chem. Eng. J.* 382, 122837–122845.
- Li, X. et al., 2020. High-efficiency degradation of organic pollutants with Fe, N co-doped biochar catalysts via persulfate activation. *J. Hazard. Mater.* 397, 122764–122774.
- Li, B. et al., 2022a. Enhancement strategies for efficient activation of persulfate by heterogeneous cobalt-containing catalysts: a review. *Chemosphere* 291, 132954–132972.
- Li, X. et al., 2022b. Kill three birds with one stone: Iron-doped graphitic biochar from biogas residues for ammonium persulfate activation to simultaneously degrade benzo[a]pyrene and improve lettuce growth. *Chem. Eng. J.* 430, 132844–132853.
- Li, M.Z. et al., 2023a. Recent status and future perspectives of ZnIn<sub>2</sub>S<sub>4</sub> for energy conversion and environmental remediation. *Chinese Chem. Lett.* 34, (7) 107775.
- Li, Y. et al., 2023b. Activation of hydrogen peroxide by molybdenum disulfide as Fenton-like catalyst and cocatalyst: Phase-dependent catalytic performance and degradation mechanism. *Chinese Chem. Lett.* 34, (2023) 107874.
- Liu, G.C. et al., 2018. Formation and physicochemical characteristics of nano biochar: insight into chemical and colloidal stability. *Environ. Sci. Tech.* 52 (18), 10369–10379.
- Liu, F. et al., 2022. Catalytic pyrolysis of lotus leaves for producing nitrogen self-doping layered graphitic biochar: Performance and mechanism for peroxydisulfate activation. *Chemosphere* 302, 134868–134876.
- Nguyen, V.T. et al., 2019. Efficient heterogeneous activation of persulfate by iron-modified biochar for removal of antibiotic from aqueous solution: a case study of tetracycline removal. *Catalysts* 9, 1–14.
- Pang, Y. et al., 2018. Preparation and application of magnetic nitrogen-doped rGO for persulfate activation. *Environ. Sci. Pollut. R.* 25, 30575–30584.
- Ren, W. et al., 2020. The intrinsic nature of persulfate activation and N-doping in carbocatalysis. *Environ. Sci. and Technol.* 54, 6438–6447.
- Song, G. et al., 2022. Tailoring biochar for persulfate-based environmental catalysis: impact of biomass feedstocks. *J. Hazard. Mater.* 424, 127663–127688.
- Strnad, S., Zemlji, L.F., 2023. Cellulose-Chitosan functional biocomposites. *Polymers* 15.
- Tang, L. et al., 2018. Enhanced activation process of persulfate by mesoporous carbon for degradation of aqueous organic pollutants: electron transfer mechanism. *Appl. Catal. B: Environ.* 231, 1–10.
- Wang, H. et al., 2019. Edge-nitrogenated biochar for efficient peroxydisulfate activation: An electron transfer mechanism. *Water Res.* 160, 405–414.
- Wang, S. et al., 2022. Development of high-performance adsorbent using KOH-impregnated rice husk-based activated carbon for indoor CO<sub>2</sub> adsorption. *Chem. Eng. J.* 437, 135378–.
- Xi, M. et al., 2021. Enhanced norfloxacin degradation by iron and nitrogen co-doped biochar: revealing the radical and nonradical co-dominant mechanism of persulfate activation. *Chem. Eng. J.* 420, 129902–129915.
- Xu, B. et al., 2016. Facile synthesis of nitrogen-doped, hierarchical porous carbons with a high surface area: the activation effect of a nano-ZnO template. *J. Mater. Chem. A* 10, 16341–16348.
- Yu, J. et al., 2019. Magnetic nitrogen-doped sludge-derived biochar catalysts for persulfate activation: internal electron transfer mechanism. *Chem. Eng. J.* 364, 146–159.
- Yu, J.F. et al., 2020a. Metal-free carbon materials for persulfate-based advanced oxidation process: microstructure, property and tailoring. *Prog. Mater. Sci.* 111, 100654–100692.
- Yu, J.F. et al., 2020b. Hierarchical porous biochar from shrimp shell for persulfate activation: a two-electron transfer path and key impact factors. *Appl. Catal. B: Environ.* 260, 118160–118172.
- Yuan, Y. et al., 2023. One-step preparation of a novel graphitic biochar/Cu<sup>0</sup>/Fe<sub>2</sub>O<sub>4</sub> composite using CO<sub>2</sub>-ambiance pyrolysis to activate peroxydisulfate for dye degradation. *J. Environ. Sci.* 125, 26–36.
- Zhang, J. et al., 2015. Effects of pyrolysis temperature and heating time on biochar obtained from the pyrolysis of straw and lignosulfonate. *Bioresour. Technol.* 176, 288–291.
- Zhang, H.X. et al., 2020. Efficient removal of organic pollutant by activation of persulfate with magnetic Co<sub>3</sub>O<sub>4</sub>/CoFe<sub>2</sub>O<sub>4</sub> composite. *Arab. J. Chem.* 13, 5332–5344.
- Zhang, S. et al., 2021. Membrane-Confined iron oxychloride nanocatalysts for highly efficient heterogeneous fenton water treatment. *Environ. Sci. Tech.* 55, 9266–9275.
- Zhong, Q. et al., 2021. Study on the nonradical pathways of nitrogen-doped biochar activating persulfate for tetracycline degradation. *Sep. Purif. Technol.* 276, 119354–119363.
- Zhu, S. et al., 2018. Catalytic removal of aqueous contaminants on N-Doped graphitic biochars: inherent roles of adsorption and nonradical mechanisms. *Environ. Sci. Tech.* 52 (15), 8649–8658.
- Zou, J. et al., 2020. Analysis of reaction pathways and catalytic sites on metal-free porous biochar for persulfate activation process. *Chemosphere* 261, 127747–127764.